Hindawi
International Journal of Chemical Engineering
Volume 2022, Article ID 4441718, 18 pages
https://doi.org/10.1155/2022/4441718

Research Article

Synthesis and Characterization of Fe_3O_4-Bentonite Nanocomposite Adsorbent for Cr(VI) Removal from Water Solution

Ngusey Adisu,[1] Subramanian Balakrishnan ,[1,2] and Haimanot Tibebe[1,2]

[1]*Department of Chemical Engineering, Addis Ababa Science and Technology University, Addis Ababa, Ethiopia*
[2]*Nanotechnology Center of Excellence, Addis Ababa Science and Technology University, Addis Ababa, Ethiopia*

Correspondence should be addressed to Subramanian Balakrishnan; bsubra05@gmail.com

Received 2 June 2022; Revised 11 August 2022; Accepted 18 August 2022; Published 8 September 2022

Academic Editor: Selvaraju Narayanasamy

Bentonite-magnetite nanocomposite adsorbent (BMNC) was made and investigated for its adsorption removal of Cr(VI) from an aqueous solution. This adsorbent was prepared by the coprecipitation method from sodium bentonite (BNa) with iron chloride solution at controlled pH and under an inert atmosphere. These adsorbents were characterized by atomic absorption spectrophotometer (AAS), Brunauer–Emmett–Teller (BET), dynamic light scattering (DLS), scanning electron microscope (SEM), Fourier transform infrared (FTIR) spectroscopy, and X-ray diffraction (XRD) analyses. Particle size of BMNC was in the range of 15 to 95 nm as per DLS. The intercalation of magnetite nanoparticles onto the bentonite clay increased its specific surface area from 142 to 177 m^2/g as per BET analysis. Experimental design optimization results in 96.5% of Cr(VI) removal from the water solution at optimized adsorption parameters viz., adsorption time of 101 min, pH of 1.95, adsorbent dose of 1.12 g/L, and initial Cr(VI) concentration of 36.2 mg/L. The results of these studies demonstrate that the BMNC performs well. Moreover, the adsorption of Cr(VI) onto the BMNC was found to be the best fit with Langmuir isotherm ($R^2 = 0.9984$) and a maximum adsorption capacity of 98 mg/g. The kinetics of the adsorption process was found to be a pseudo-second-order model ($R^2 = 0.9912$). The BMNC also showed favourable reusability for adsorbate Cr(VI) ions removal from the water solution.

1. Introduction

The quality of potable water has become increasingly sensitive worldwide and allocation of water resources is among the most critical global issues. Nowadays, different toxic organic, inorganic, and microbial contaminants have been recognized at basic levels in all water resources. Large water contamination is due to the large usage of organic solvents, hazardous industrial chemicals, heavy metals, textile dyes, detergents, soaps, fertilizers, pesticides, herbicides, pathogens, and paint pigments, which all find their way into water resources [1, 2]. Generally, contaminants like various heavy metals and dyes exist stable in the aqueous medium, which also causes serious damage to the water ecosystem, its flora-fauna, and the environment [3]. Some of the heavy metal contaminants are chromium, zinc, lead, nickel, platinum, silver, and cadmium ions [4]. Their concentration in the environment has dramatically increased to a dangerous level due to extensive industrial activities such as electroplating, anodizing-cleaning, etching, and milling [5]. Heavy metals could enter and accumulate in the human body through the food and ecological chain and cause bioaccumulation, which leads to chronic health disorders such as cancer, kidney failure, liver damage, brain damage, and bone softening [6]. In recent times, the removal of toxic heavy metal ions from water supplies and wastewater has been a core interest for many researchers and scientists throughout the world [7]. Dil et al. [8] have reported 98.84% of Azure B dye adsorption removal from aqueous solution by utilizing novel hybrid nanocomposite catalysts based on carbon nanotube, zinc oxide, zinc, and nickel-phosphorus metalloid.

Toxic metal ions are released from the leather chrome tanning process, which cannot be easily removed by the ordinary treatment process. Effluents from the tanning processes are mainly characterized by high organic loading, salinity, and specific pollutants such as chromium ions [9]. Chromium is found in two stable oxidation states Cr(III) and Cr(VI). Trivalent chromium is a micronutrient for its catalytic role in protein metabolism in animals and plants, whereas hexavalent chromium Cr(VI) ion is very toxic to many lives, particularly humans. The human body can convert harmful Cr(VI) into Cr(III) ions to some extent. Anything beyond 0.003 ppm level of Cr(VI) ion chronic exposure causes serious health issues [10]. Cr(III) compound is widely used in leather tanning, fungicides, dyes, paints, ceramics, stainless steel, electroplating, and glass industries [11]. The presence of Cr(III) in an environment beyond the permissible limit of 0.05 mg/L and long-term exposure can cause serious health problems for man and other living beings [12]. Presence of strong oxidants or in alkaline conditions, the Cr(III) gets easily oxidized into harmful Cr(VI) in soil or water. Cr(VI) ion can cause critical problems like inhibition of plant growth, genetic mutation, diarrhoea, nose ulcers, running nose, cough, breathing difficulty, asthma, kidney and liver failure, and cancer [13, 14].

Industrial effluents like wastewater must be properly treated to the permissible limit before being discharged into the environment [6]. Many conventional methods have long been applied for the removal of Cr(VI) ions from contaminated waters such as chemical precipitation, membrane separation, ion exchange, electrochemical treatment, and advanced oxidation processes [15, 16]. However, these processes are often costly, inefficient, resulted in toxic by-products, and energy intensive [17–19]. Amongst catalytic adsorption, removal of Cr(VI) ion has become an effective technique due to its low cost, locally available materials, high efficiency, and easier remediation of the used products. The adsorption process directly depends on the type of adsorbent and its properties. The adsorbents should be cheap, environmentally friendly, and efficient. Several adsorbents such as activated carbon, zeolite, chitosan, hydrogel, and clays have been studied to remediate toxic heavy metals from soil and wastewater [7, 19].

In the last few decades, magnetite (Fe_3O_4) nanoparticles have attracted the attention of researchers in the field of environmental remediation. Additionally, magnetite can be easily separated and collected by an external magnetic field after the adsorption process. Applications of magnetite nanoparticles are mainly due to their much better adsorption reduction activities than their traditional macro counterparts [20]. Also, magnetite nanoparticles possess high adsorption capacity and a fast adsorption rate [21]. These extraordinary advantages are specifically useful for the reusability of magnetite nanoparticles [22]. In recent years, many efforts have been made to prepare adsorbent materials by incorporating magnetite nanoparticles [3, 21–24].

Clay is a natural silicate mineral that has been widely used as an important sorbent in the removal of heavy metals because of being abundant, economical, and environmentally friendly. Amongst, bentonite clay is a naturally abundant and cheap mineral in Ethiopia and around the globe; it has been extensively used in many industrial applications including wastewater treatment [25]. Bentonite clay principally contains montmorillonite. Sodium bentonite is high swelling, while calcium bentonite is low swelling clays [26]. Even though bentonite clay has a high specific surface area, cation exchange capacity, and other advantages, it needs modification for better adsorption and affinity to heavy metal ions [27]. Ashour and Tony [28] used acid and thermally modified clays and reported 66% Cr(VI) removal efficiency from an aqueous solution with 14.3 mg/g adsorption capacity at an equilibrium time of 90 min. Castro-Castro et al. [4] modified the clay using a cationic surfactant of hexadecyltrimethylammonium bromide and reported the removal of 93.2% of Cr(VI) from an aqueous solution with 10.04 mg/g adsorption rate at an equilibrium time of 120 min. Jia et al. [29] reported 87.6% Cr(VI) removal from aqueous solution by chitosan/bentonite adsorbent at an equilibrium time of 1.5 hr. The challenges to natural and modified bentonite are the difficulty in separation of the adsorbent from the solution after the adsorption process. It involves very special techniques to separate the adsorbent from the solution due to the clay's low mechanical stability and high dispersion [13]. So, modification of the bentonite clay that enhances its absorptivity and filterability is the focus of this research. In this line, bentonite-magnetite nanocomposite adsorbent was prepared by coprecipitation method to remove Cr(VI) ions from water solution formulation targeting low-cost, abundance, high specific surface area, adsorption capacity, easy-to-handle, and filterable properties.

2. Materials and Methods

2.1. Chemicals and Equipment. Analytical-grade chemicals and reagents were used. Iron (III) chloride hexahydrate ($FeCl_3.6H_2O$, purity 99%), and iron (II) chloride tetrahydrate ($FeCl_2.4H_2O$, purity 99%) were used to prepare magnetite nanoparticles. Sodium hydroxide (NaOH, 99% pure) was used to intercalate the magnetite nanoparticles by coprecipitation method and also for pH adjustment. Hydrochloric acid (HCl, 99% pure) was used to adjust the pH of the solutions. Sodium chloride (NaCl, 99% pure) was used to prepare sodium bentonite from purified calcium bentonite. Potassium dichromate ($K_2Cr_2O_7$, purity 99%) was used to prepare Cr(VI) ion solution. Diphenyl carbazide (DPC) (99% pure) was used as a selective chelating reagent in UV-vis spectrophotometer analysis to determine Cr(VI) ion concentration. Acetone (C_3H_6O, 99.5% pure) was used to dissolve the DPC.

2.2. Raw Bentonite Treatments and Sample Preparation

2.2.1. Bentonite Size Reduction. The raw clay, principally calcium bentonite, was sourced from the Gewane area (Afar region, Ethiopia) and used for this study to prepare a synthetically modified adsorbent. The bulk raw bentonite was subjected to size reduction using a jaw crusher followed

by a disk mill to make it ready for the pretreatment process. The bentonite powder was sieved using ISO 3310-1 sieving machine to get a 63 μm particle size.

2.2.2. Pretreatment and Sodium Bentonite Preparation. The crushed sample was purified by washing it with distilled water three times to remove the adhered impurities and soluble salts from the powdered clay and centrifuged to recover it. The filtered clay was then dried in an oven and incubator dryer (PRI/150/A) for 24 hours at 105 °C to remove the moisture. Then, the dried clay sample was ground and activated by soaking 10 g in 100 ml of 1 M NaCl solution. The activation process was performed by stirring vigorously for 6 hours to get a sodium ion intercalation saturated bentonite. Then, the sodium bentonite was washed with distilled water four times until neutral pH was noticed in the filtrate. Again, the sodium bentonite (BNa) was dried at 105 °C for 12 hours; then, it was ground and sieved to obtain 63 μm particle size and stored in glass vials.

2.3. Synthesis of Bentonite-Magnetite Nanocomposite Adsorbent. The method for the synthesis of bentonite-magnetite nanocomposite adsorbent by coprecipitation synthesis method was adapted from a previous study with minor modifications [3]. A solution of iron (II) and iron (III) was prepared by dissolving 1 g of $FeCl_2{\cdot}4H_2O$ and 2.5 g $FeCl_3{\cdot}6H_2O$ in 150 ml of distilled water (1 : 2 molar ratio). Subsequently, intercalation of precipitation with BNa was performed. The purified BNa powder was added to the prepared iron chloride solutions by varying the amount of clay (1–4 g) and reaction time (1–4 hrs). Later, the solution was subjected to precipitation by adding 1 M NaOH solution drop by drop until a black precipitate was observed. The reaction was carried out at 85 °C and 10 pH under a nitrogen gas inert atmosphere. The intercalation coprecipitation process was performed using a hot plate stirrer at 300 rpm speed. Then, the resulting solution was allowed to settle down at room temperature and then filtered using an external magnet. The bentonite-magnetite nanocomposite was washed several times with distilled water to remove unfixed iron oxide compounds. The washing process was performed until the neutral pH of the filtrate was achieved. The synthesized nanocomposite adsorbent was dried in an oven at 105 °C for 24 hours. The dried adsorbent was milled using a disk mill, sieved to obtain 63 μm particle size, and stored in dry glass vials until the adsorption experiments. Hereafter, this synthesized bentonite-magnetite clay will be referred to as nanocomposite adsorbent and also abbreviated as BMNC.

2.4. Characterization of Adsorbents. Complete silicate analysis was carried out to find out the chemical composition of the BNa and BMNC adsorbent samples by atomic absorption spectrophotometer (AAS). The size distribution and hydrodynamic diameter of the BMNC were determined using dynamic light scattering (DLS) (Malvern zeta sizer, ZEN3600). The specific surface area of the BNa and BMNC was estimated by Brunauer–Emmett–Teller (BET) method based on the adsorption and desorption isotherms of nitrogen gas at room temperature and an atmospheric pressure of 700 mm Hg using the SA-9600 Horiba surface area analyzer. The functional group characteristics of BNa and BMNC samples were analyzed by the Fourier transform infrared spectroscopy (FTIR) (Thermo Scientific iS50 ABX model) in a wave number range of 4000 to 400 cm^{-1}. The surface morphology of the adsorbents was examined using the scanning electron microscope (SEM) (FEI, INSPECT-F50, Germany) at the operating conditions of 10 kV power, 3000× magnification, 10 μm scale, 10 mm working distance, and vacuum. The crystal structure of both adsorbents was studied using an X-ray diffraction (XRD-7000, Shimadzu, Japan) machine operating at 40 kV and 40 mA in the range of 2θ of 10–80° with a scanning rate of 10 min^{-1} and point of zero charge (PZC) of the adsorbents was determined using the salt addition method.

2.5. Design of Adsorption Experiments and Optimization. The adsorption of Cr(VI) onto both adsorbents was carried out in a batch process. A stock solution of Cr(VI), 1000 mg/L was prepared by dissolving 2.83 g of $K_2Cr_2O_7$ in one liter of distilled water. Initially, one variable at a time (OVAT) experimental design was performed to determine the effects of different operating conditions on the Cr(VI) ion adsorption capacity by both the adsorbents. The interaction effects of the independent parameters were studied using the response surface methodology (RSM)-based central composite design (CCD) [30]. Design-Expert-12 software was used for the RSM-CCD study. Based on OVAT results, four adsorption parameters viz., pH, adsorption time, initial Cr(VI) ion concentration, and adsorbent dose were selected for adsorption process optimization.

2.5.1. Individual Parameter Effects on the Adsorption Process. Preliminary OVAT experiments were conducted by varying the adsorption time (30–210 min), pH (1–7), adsorbent dose (0.5–3.5 g/L), and initial Cr(VI) ion concentration (20–140 mg/L). In these experiments, the effect of one variable was studied by fixing all other variables at constant values. The adsorption capacity of the BMNC was studied by varying initial Cr(VI) ion concentrations of 10, 20, 30, 40, and 80 mg/L by fixing pH at 2, time at 90 min, and adsorbent dose at 0.1 g/L [28]. Similarly, the effect of a range of individual parameters on the Cr(VI) ion adsorption by both adsorbents was examined as listed in Table 1.

The adsorption experiments were conducted in 200 ml of conical flasks using a magnetic hot plate stirrer at 300 rpm. After the adsorption process was completed, the mixture was taken out and filtered using Whatman filter paper for the BNa and magnetic separation for the BMNC. The filtrate was then analyzed for Cr(VI) ion concentration by UV spectrophotometer (JASCO V-770, Japan) at 540 nm maximum wavelength [31, 32]. All OVAT experimental results are averaged out of triplicate experiments with an error bar in the plotted graphs. The percentage of Cr(VI) removal efficiency by adsorbents was calculated using the following equation:

Table 1: Parameters and their levels for OVAT analysis.

Parameters	Unit	Level						
Adsorption time	Min	30	60	90	120	150	180	210
pH	—	1	2	3	4	5	6	7
Adsorbent dose	g/L	0.5	1	1.5	2	2.5	3	3.5
Cr(VI) ion initial concentration	mg/L	20	40	60	80	100	120	140

Table 2: Independent parameters and their coded levels for CCD experiments.

Parameters	Symbol	Unit	Level		
			Low (−1)	Medium (0)	High (+1)
Adsorption time	A	Min	60	90	120
PH	B	—	1.5	2	2.5
Adsorbent dose	C	g/L	1	1.25	1.5
Cr(VI) ion initial concentration	D	mg/L	25	40	55

$$\text{Removal efficiency}\,(\%) = \frac{(Ci - Cf)}{Ci} * 100, \tag{1}$$

where Ci and Cf are initial and final Cr(VI) concentrations (mg/L), respectively.

2.5.2. Study of Parameters' Interaction Effect and Model Evaluation Using RSM-CCD. Based on the analysis of the preliminary experiments by OVAT, four parameters with three levels were selected for the study of interaction effects and the model evaluation, as listed in Table 2.

Duplicate experiments were conducted and average values were taken for all experiments. A mathematical model was developed to relate the independent parameters with removal efficiency response. Regression analysis was performed for the quadratic model, as shown in the following equation:

$$\begin{aligned}\text{Removal efficiency}\,(\%) = {} & \beta + a_1 A + a_2 B + a_3 C + a_4 D \\ & + b_1 AB + b_2 AC + b_3 AD + b_4 BC,\end{aligned} \tag{2}$$

where β is an intercept constant, a_1–a_4 are coefficients of main effects, b_1–b_6 are coefficients of parameters interaction, c_1–c_4 are coefficients of quadratic effects, and A–D are experimental variables.

2.5.3. Optimization of Process Parameters and Statistical Analysis. Optimization of process variables (adsorption time, pH, adsorbent dose, and initial Cr(VI) ion concentration) was conducted using Design-Expert-12 software to obtain the optimum response of Cr(VI) removal by the BMNC. The performance and significance of the model were evaluated using a statistical analysis tool (ANOVA) in terms of coefficient of determination (R^2), probability (p value), and Fisher value (F value). Triplicate experiments were conducted utilizing optimized parameters to validate the model and the result is compared with the predicted one.

2.6. Adsorption Isotherms and Kinetics Studies. Well-known model isotherms and kinetics were examined to understand the adsorption mechanism and kinetics of Cr(VI) ion adsorption onto the BMNC. To study these, 0.112 g adsorbent was added to 100 ml of Cr(VI) solution of 36.2 mg/L concentration and pH of 1.95 in a flask of 250 ml. The solution was stirred using a magnetic stirrer at 300 rpm and at room temperature. The filtrate of the adsorption process was analyzed to measure the remaining Cr(VI) ion concentration at the given time using UV-visible spectroscopy.

2.6.1. Adsorption Isotherms. An equilibrium relationship between the amounts of Cr(VI) ion adsorbed onto adsorbents was established through adsorption isotherms models. In this study, Langmuir, Freundlich, and Temkin isotherm models were examined to fit the experimental data. The adsorption capacity (qe) of the BMNC at equilibrium Cr(VI) concentration was calculated by the following equation [33]:

$$qe = \frac{(Ci - Ce) * V}{m}, \tag{3}$$

where qe (mg/g) is the amount of Cr(VI) ion adsorbed at equilibrium, Ci (mg/L) is the initial concentration of Cr(VI), Ce (mg/L) is the concentration of Cr(VI) at equilibrium, V (L) is the volume of the Cr(VI) solution, and m (g) is the mass of the adsorbent.

The Langmuir isotherm model is derived by considering the adsorption process as a monolayer surface that contains a limited number of adsorption sites with uniform strategies and no transmigration on the plane of the surface [34]. The Langmuir equation is written in the linear form as follows:

$$\frac{Ce}{qe} = \frac{1}{K_L\, qm} + \frac{Ce}{qm}, \tag{4}$$

where Ce is the concentration of the adsorbate at equilibrium (mg/L), qe is the amount of the adsorbate at equilibrium (mg/g), qm is maximum adsorption capacity (mg/g), and K_L is Langmuir rate constant (L/mg).

Freundlich isotherm model is an empirical equation used for multilayer and heterogeneous adsorption sites [35]. This is the earliest known model that describes a non-ideal and reversible adsorption process. This empirical model can be applied to multilayered adsorption, where the heat of adsorption and affinity are unevenly distributed over the nonuniform surface [36]. The linear form of the Freundlich isotherm equation is written as follows:

$$\ln qe = \ln Kf + \frac{1}{n}\ln Ce, \quad (5)$$

where qe is the amount of Cr(VI) adsorbed at equilibrium, Ce is Cr(VI) ion concentration in the solution, Kf is the Freundlich constant, and n is the adsorption intensity.

The Temkin adsorption isotherm model is used to indicate the indirect effect of adsorbent and adsorbate interactions on the process of adsorption. It estimates that the heat of the layer adsorption is in a linear decrease as a result of an increase in surface coverage. The linear Temkin expression is represented as follows [28, 37]:

$$qe = B\ln(KT) + B\ln(Ce), \quad (6)$$

where B is described as ($B = RT/b$) and it indicates the heat of adsorption, T is the absolute temperature (298 K), R is the universal gas constant (8.314 J·mol^{-1}/K), and K_T is the equilibrium binding constant.

2.6.2. Kinetics Studies. Pseudo-first-order and pseudo-second-order equations were applied to model kinetics of Cr(VI) ion adsorption onto the BMNC to investigate the rate of adsorption and controlling mechanisms of the adsorption process such as mass transfer and chemical reaction. These different experiments were conducted by varying the adsorption time at 20, 40, 60, 80, 100, 120, and 140 min. The amount of Cr(VI) ion adsorbed for time (qt) onto the BMNC was calculated using the following equation [38]:

$$qt = \frac{(Ci - Ct) * V}{m}, \quad (7)$$

where qt (mg/g) is the amount of Cr(VI) ion adsorbed at time t, Ci (mg/L) is the initial Cr(VI) ion concentration, Ct (mg/L) is the final Cr(VI) ion concentration at a time t, and V (L) and m (g) are the volumes of solution and adsorbent dose, respectively.

The pseudo-first-order kinetic model assumes that the rate of change of the solute uptake with time is directly proportional to the difference in the saturation concentration and amount of solid uptake with time [15]. The fitness of the pseudo-first-order kinetic model was tested using the following linearized equation [38]:

$$Ln(qe - qt) = \ln(qt) - k_1 t, \quad (8)$$

where qe and qt are the amount of adsorbate adsorbed at equilibrium and time t, respectively (mg/g), and k_1 is the rate constant (min^{-1}). The values of qe and k_1 were determined from the intercept and slope of the graph of ln(qe–qt) versus t.

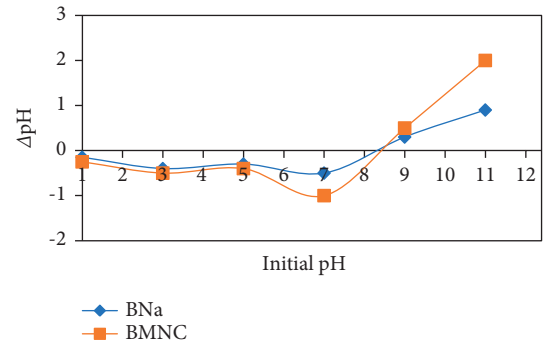

Figure 1: pH-dependent zero charges of bentonite (BNa) and the nanocomposite adsorbent (BMNC).

The pseudo-second-order kinetic model suggests that physisorption and chemisorption are involved in the adsorption of Cr(VI) ions onto the BMNC [15, 38]. The data used to fit the model are represented in the following equation:

$$\frac{t}{qt} = \frac{1}{K_2\, qe^2} + \frac{t}{qe}, \quad (9)$$

where K_2 is the pseudo-second-order adsorption rate constant. The values of k_2 and qe can be evaluated from the slope and intercept of the graph of t/qt versus t.

The intraparticle diffusion kinetic model, which was proposed by Weber and Morris, can be described by the following equation [33, 37:

$$q_t = K_d t^{0.5} + C, \quad (10)$$

where K_d (mg/g.min$^{0.5}$) is the intraparticle diffusion rate constant and C (mg/g) is the intercept.

2.7. Reusability of the BMNC Adsorbent. The BMNC was used to determine its recycling performance. This experiment was conducted at 1.95 pH, 101 min adsorption time, 1.12 g/L adsorbent dose, and 36.2 mg/L initial Cr(VI) concentration. Regeneration of the adsorbent was carried out using 0.5 M of NaOH solution. After washing the adsorbent with NaOH solution, it was rinsed with distilled water copiously and the adsorbent was collected using an external magnet. Cr(VI) ion adsorption and regeneration were repeated for six consecutive cycles. Results reported an average out of duplicate experiments in all six cycles.

3. Results and Discussion

3.1. Characterization of BNa and BMNC

3.1.1. Point of Zero Charge (PZC). PZC is an important property of an adsorbent that indicates the charge neutrality of the adsorbent's surface at a specified pH. The PZC of the BNa and the BMNC were determined from the common intersection point of the curves with a straight line. A graph of ΔpH versus initial pH was plotted successfully as shown in the following Figure 1. It can be observed that the PZC is almost 8.5 for BNa and BMNC adsorbents. This suggests that

Table 3: Chemical composition of bentonite (BNa) and the nanocomposite adsorbent (BMNC) using AAS.

Parameters	SiO_2	Al_2O_3	Fe_2O_3	CaO	Na_2O	MgO	K_2O	MnO	P_2O_5	H_2O	TiO_2	LOI
BNa (wt.%)	57.1	10.4	7.14	4.66	4.02	4.5	2.04	0.08	0.11	1.52	<0.01	7.67
BMNC (wt.%)	58.1	8.72	15.4	2.14	6.2	2.01	0.25	0.01	0.005	1.8	0.001	5.57

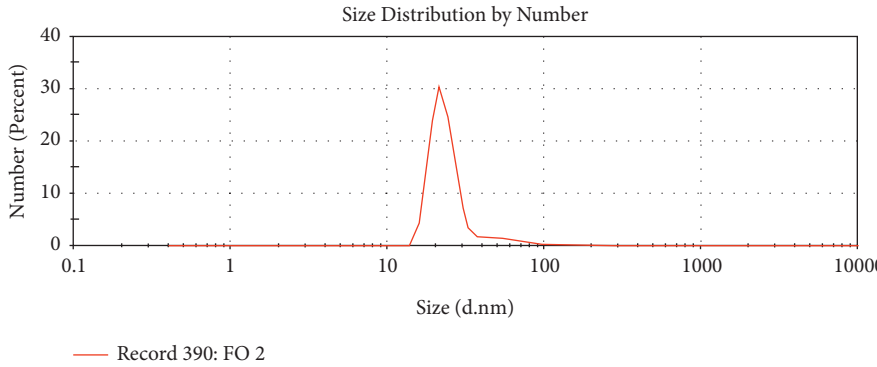

Figure 2: Particle size distribution of the nanocomposite adsorbent (BMNC).

the presence of intercalated magnetite nanoparticles onto bentonite clay did not change its charge properties but rather improve its surface area and morphology as confirmed by BET and SEM analyses. A similar result was obtained for both adsorbents [39]. When the solution pH is below to pH of PZC, the adsorbent's surface has a net positive charge and is favourable for anionic exchange. If the solution pH is above to pH of PZC, the adsorbent's surface has a net negative charge and is favourable for cationic exchange.

3.1.2. Chemical Composition Analysis. The major and minor oxides of BNa and the BMNC from AAS are listed in Table 3. The analysis confirmed that the adsorbent clays are rich in SiO_2, while the BMNC consists of nearly two times more Fe than BNa. A similar result was reported for iron oxide-modified bentonite [40]. After activation with NaCl and subsequently, iron oxide intercalation shows a slight increase in SiO_2 and a decrease in Al_2O_3. After these modifications, an increase in Na_2O and a decrease in CaO contents are indications of the conversion of calcium bentonite into BNa. A study showed that chemical composition of bentonite consists of 52.6% SiO_2, 15.3% Al_2O_3, 11.9% Fe_2O_3, 3.22% Na_2O, 1.4% CaO, 1.62% TiO_2, 2.75% MgO, 9.8% LOI, and 0.06% P_2O_5 [41]. Another study showed that the Australian bentonite is composed of 56% SiO_2, 16% Al_2O_3, 4.6% Fe_2O_3, 2.9% Na_2O, 0.9% CaO, 3.3% MgO, 5.7% LOI, 0.4% K_2O, and 10% H_2O [42].

3.1.3. Particle Size Analysis by DLS. Nanoscale materials are defined as the range of 1–100 nm in size [43]. DLS result shown in Figure 2 indicates that the average size distribution of the BMNC is in the range of 15 nm to 95 nm and the average is around 30 nm. Hence, this is a nanomaterial.

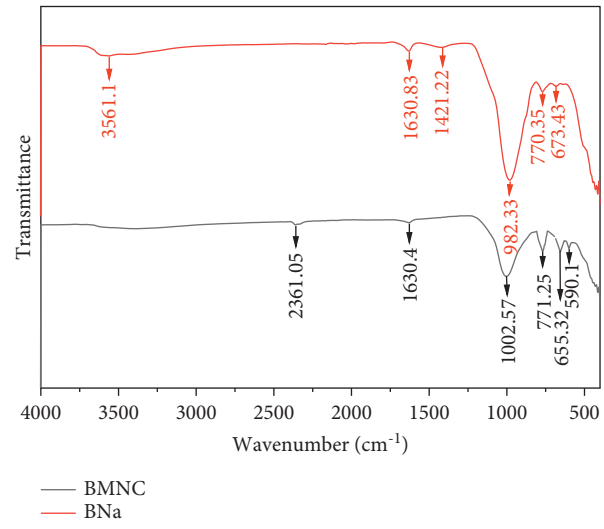

Figure 3: FTIR spectra of bentonite (BNa) and the nanocomposite adsorbent (BMNC).

3.1.4. BET Analysis. BET analysis showed that the BNa has a specific surface area of 142 m^2/g, and the BMNC has a specific surface area of 177.3 m^2/g. Interestingly, the intercalation of the magnetite nanoparticles into bentonite increased its specific surface area and hence more favourable for the adsorption process. A study has reported 35.8 m^2/g as a specific surface area for bentonite [24]. Yet another study reported 59.9 m^2/g as a specific surface area for bentonite [4]. Similarly, Song et al. have reported 100.2 m^2/g as a specific surface area for the nanocomposite adsorbent [21]. The specific surface areas of both BNa and BMNC are in a similar order. The coprecipitation of magnetite nanoparticles with BNa leads to an increase in the specific surface area, which

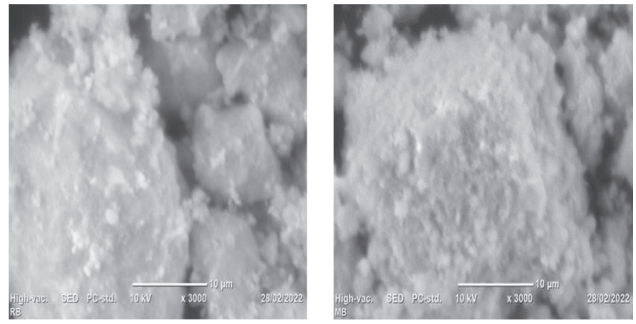

(a) (b)

Figure 4: SEM images of (a) bentonite (BNa) and (b) nanocomposite adsorbent (BMNC).

could enhance the adsorption capacity of the resultant adsorbent [43].

3.1.5. FTIR Analysis. The FTIR spectra (Figure 3) contribute to an understanding of the chemical structure, bonding, and absorptivity characteristics of adsorbents. The structural hydroxyl groups and the water molecules are observed in the region between 3561 and 1631 cm^{-1} for these adsorbents; whereas, the main silicate absorption bands are observed between 1200 and 550 cm^{-1}. Similar results are reported by others [23, 44]. Broadband was observed at 3561 cm^{-1} due to the O-H stretching vibrations of the structural hydroxyl (Si-OH) groups of the clay sheets and the band at 1631 cm^{-1} indicates the angular deformation of the H-O-H bond of absorbed water molecules in silicate interlayer [44]. The characteristic sharp band at 982 cm^{-1} is assigned to the stretching vibration of the tetrahedral layer Si-O group [21]. Two weak and sharp bands observed at 770 cm^{-1} and 550 cm^{-1} are assigned to Si-O-Al and Si-O-Si stretching vibrations [41]. BMNC shows slight shift in some absorption peak positions. For instance, there is an absorption peak at 982 cm^{-1} in the case of BNa corresponding to the Si-O group; but this peak is shifted to 1003 cm^{-1} in the case of BMNC. This change could be due to the interaction of the magnetite nanoparticles with the clay sheets. The dwarf peak for BMNC at 2361 cm^{-1} was attributed to the C-O-H bond. This may be due to the catalytic absorption of CO_2 during the coprecipitation synthesis of the BMNC [45]. Another peak that occurred at 655 cm^{-1} is assigned to Fe-O stretching and is proof of magnetite nanoparticles in BMNC [46].

3.1.6. SEM Analysis. The surface morphology of these clay adsorbents is shown in Figure 4. Micrograph 4(a) indicates that the surface structure is smooth and porous in the case of BNa; whereas, the SEM morphology of BMNC shows highly porous and the presence of magnetite nanoparticles on the surface. Micrographs of the latter also show small and spherical particles, which increased the specific surface area corroborating the BET surface area analysis results. The formation of spherical particles could enhance the intercalation of magnetite nanoparticles onto bentonite clay [33].

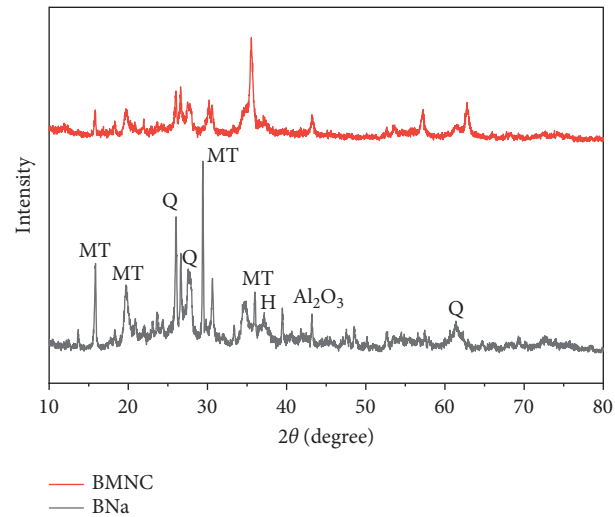

Figure 5: XRD diffraction of bentonite (BNa) and nanocomposite adsorbent (BMNC).

3.1.7. X-Ray Diffraction (XRD) Analysis. The XRD diffraction peaks for the BNa appeared at 2Θ angles of 15.8°, 19.9°, 26°, 26.7°, 27.9°, 29.8°, 30.5°, 34.5°, 34.7°, 39.5°, 43.2°, 52.7°, and 61.6° are shown in Figure 5. The presence of montmorillonite (MT) is observed at diffraction peaks of 15.8°, 19.9°,29.8°, 34.7°, and 39.5° [21]. The data also showed the presence of Al_2O_3 and hematite (H) at diffraction angles of 43.2° and 34.5°, respectively [44]. The spectra of both BNa and BMNC clays are almost similar, but intensities of some peaks differ and at the same time one or two new peaks appear and disappear in the case of BMNC, which indicates almost similar crystal structure and also intercalation of magnetite nanoparticles into BNa. A strong peak that appeared at 35.55° is also due to intercalated magnetite nanoparticles in bentonite clay.

3.2. Design of Experiments and Adsorption Optimization

3.2.1. Individual Parameter Effects on Adsorption Process. The preliminary OVAT adsorption optimization results are discussed by varying independent parameters such as pH from 1–7, adsorption time from 30–210 min, the adsorbent

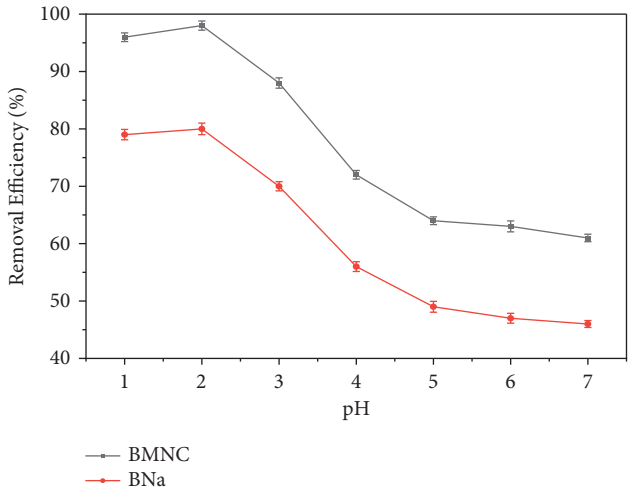

Figure 6: Effect of pH on adsorption of Cr(VI) ion by bentonite (BNa) and nanocomposite adsorbent (BMNC).

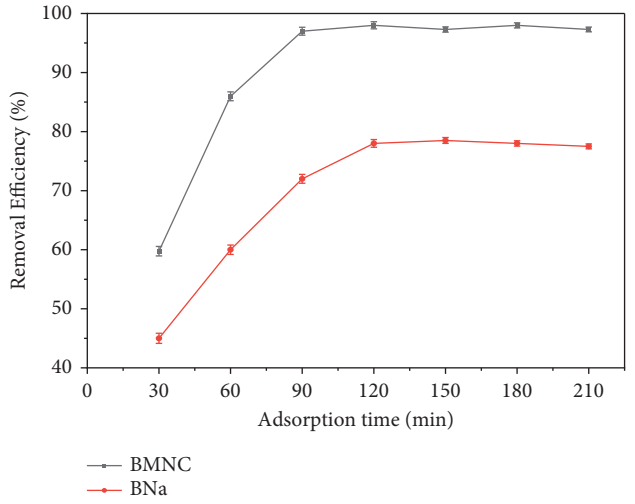

Figure 7: Effect of adsorption time on adsorption of Cr(VI) ion by bentonite (BNa) and nanocomposite adsorbent (BMNC).

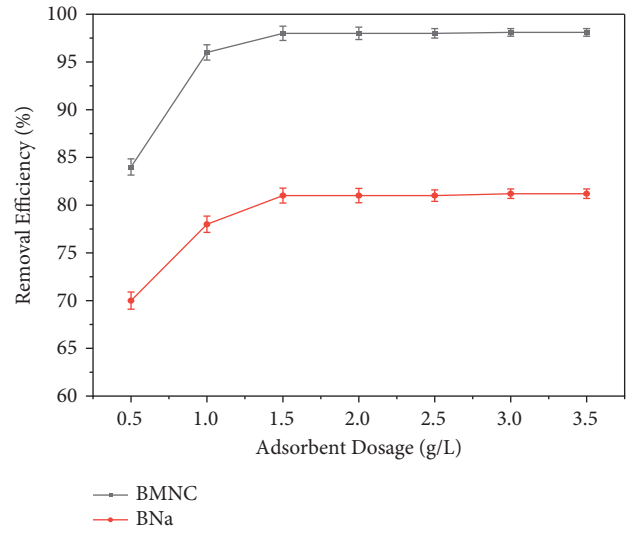

Figure 8: Effect of adsorbent dose on Cr(VI) removal efficiency by bentonite (BNa) and nanocomposite adsorbent (BMNC).

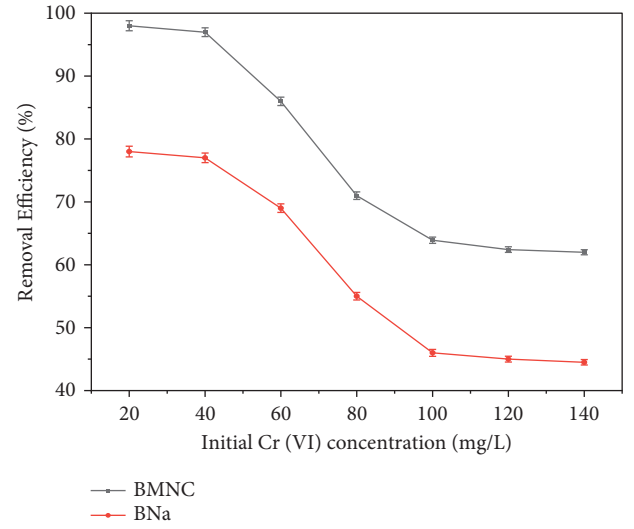

Figure 9: Effect of initial concentration on adsorption of Cr(VI) by bentonite (BNa) and nanocomposite adsorbent (BMNC).

dose from 0.5–3.5 g/L, and Cr(VI) ion initial concentration from 20–140 mg/L.

Effect of pH of Solution. Cr(VI) ion adsorption experiment was performed by varying the solution pH of 1, 2, 3, 4, 5, 6, and 7, at a constant adsorption time of 90 min, adsorbent dose of 1.25 g/L, and Cr(VI) ion initial concentration of 40 mg/L. As shown in Figure 6, maximum Cr removal efficiency is recorded as 80% by the BNa at pH 2 and it decreased to 47% as the pH of the solution increased to 6; thereafter, the removal levels off. Similarly, the Cr(VI) removal efficiency by the BMNC is recorded as 98% at pH 2 and decreased to 54% as the pH increased to 6. This is because, at a high pH, Cr(VI) ions precipitate in the form of hydroxides. Consequently, Cr(VI) ion concentration decreases in the bulk solution, thereby affecting the adsorption [22]. The adsorbent's surface is negatively charged at these high pH levels and is also a reason behind the decrease in adsorption. The other reason for the decrease in adsorption is that Cr ions exist in various forms such as dichromate ($Cr_2O_7^{2-}$), hydro chromate ($HCrO_7^-$, H_2CrO_4), and chromate ($Cr_2O_7^{2-}$) in acidic media [3, 33]. In the pH range of 2 to 6, Cr(VI) ions have two dominant forms of $Cr_2O_7^{2-}$ and $HCr_2O_7^-$, which can be converted to CrO_4^{2-} by increasing the pH of the solution [22]. The dominant form of Cr(VI) is $HCrO_4^-$ with low adsorption energy and smaller ionic size compared to $Cr_2O_7^{2-}$ [33]. Thus, smaller ionic species can easily penetrate the adsorbent as it requires less energy to diffuse.

Effect of Adsorption Time. The adsorption contact time varied from 30, 60, 90, 120, 150, 180, and 210 min at the fixed pH of 2, adsorbent dose of 1.25 g/L, and initial Cr ion

Table 4: Experimental design matrix generated by RSM-CCD for Cr(VI) ions removal using the nanocomposite adsorbent.

Run	A: adsorption time (min)	B: pH	C: adsorbent dose (g/L)	D: initial concentration (mg/L)	Removal efficiency (%)	
					Actual	Predicted
1	60	1.5	1.5	55	85.7	85.5
2	120	2.5	1	25	90.7	90.7
3	90	1	1.25	40	90.7	90.5
4	120	2.5	1.5	25	92.2	92.6
5	90	2	1.25	40	96.3	96.5
6	120	2.5	1	55	83.3	83.1
7	90	3	1.25	40	80.5	80.4
8	90	2	1.25	40	96.6	96.5
9	120	1.5	1.5	55	89	89.5
10	60	1.5	1	25	96.2	95.6
11	30	2	1.25	40	82.2	82.5
12	60	1.5	1.5	25	93.2	93.8
13	60	2.5	1.5	25	89.4	89.1
14	90	2	1.25	40	96.5	96.5
15	120	1.5	1.5	25	93.2	93.3
16	90	2	0.75	40	90.5	91
17	90	2	1.75	40	93.5	92.7
18	150	2	1.25	40	89.5	88.9
19	90	2	1.25	10	97.9	97.9
20	120	1.5	1	25	94.1	94.2
21	60	2.5	1	55	76.5	76.3
22	90	2	1.25	40	96.7	96.5
23	90	2	1.25	40	96.8	96.5
24	120	2.5	1.5	55	86.3	86.8
25	60	2.5	1.5	55	78.6	78.9
26	90	2	1.25	40	96.4	96.5
27	60	1.5	1	55	85.5	85.6
28	120	1.5	1	55	88.5	88.6
29	60	2.5	1	25	88.3	88.2
30	90	2	1.25	70	82.5	82.1

Table 5: Analysis of variance (ANOVA) for the quadratic model.

Source	Sum of squares	Df	Mean square	F value	p value	
Model	1031.64	14	73.69	347.90	<0.0001	Significant
A	61.79	1	61.79	291.74	<0.0001	
B	152.66	1	152.66	720.75	<0.0001	
C	4.69	1	4.69	22.14	0.0003	
D	373.43	1	373.43	1763.06	<0.0001	
AB	14.96	1	14.96	70.62	<0.0001	
AC	0.9555	1	0.9555	4.51	0.0507	
AD	19.34	1	19.34	91.30	<0.0001	
BC	7.52	1	7.52	35.51	<0.0001	
BD	3.87	1	3.87	18.28	0.0007	
CD	2.97	1	2.97	14.01	0.0020	
A^2	200.77	1	200.77	947.89	<0.0001	
B^2	211.11	1	211.11	996.68	<0.0001	
C^2	37.42	1	37.42	176.67	<0.0001	
D^2	72.03	1	72.03	340.07	<0.0001	
Residual	3.18	15	0.2118			
Lack of fit	2.99	10	0.2992	4.07	0.0654	Not significant
Pure error	0.1853	5	0.0371			

concentration of 40 mg/L [1]. The rapidity of the process in the initial stage is due to the large active surface area available for metal ions adsorption [33]. Thus, the adsorption level increased from 43 to 78% as the time increased from 30 to 120 min for BNa clay. The Cr(VI) adsorption was increased from 55 to 97% for BMNC as the

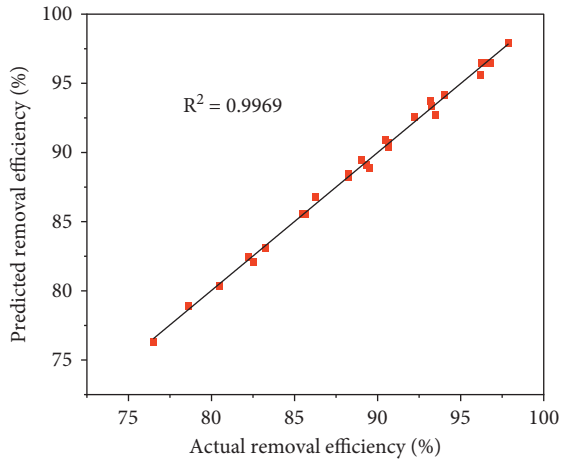

Figure 10: Experimental and predicted Cr(VI) ion removal efficiency by the model for the nanocomposite (BMNC) adsorbent.

time increased from 30 to 90 min. As shown in Figure 7, the magnetite intercalation modification has successfully increased Cr(VI) adsorption level; the equilibrium contact time is also reduced from 120 min for BNa to 90 min in the case of BMNC.

Effect of Adsorbent Dose. Cr(VI) ion adsorption level was studied for various adsorbent doses viz., 0.5, 1, 1.5, 2, 2.5, 3, and 3.5 g/L at constant pH of 2, adsorption time 90 min, and initial Cr ion concentration of 40 mg/L. As shown in Figure 8, the adsorbent dose is increased from 0.5 to 1.5 g/L, and the removal efficiency was increased rapidly from 70 to 81% for the BNa and from 84 to 98% for the BMNC. These results are because under constant metal ion concentrations, increasing the adsorbent dose increases the adsorption rate due to the increased available number of active sites in the adsorbent [3, 45]. The Cr(VI) removal efficiency levels off beyond the 1.5 g/L dose for both adsorbents.

Effect of Cr(VI) Ion Concentration. Cr(VI) ion concentrations were varied viz., 20, 40, 60, 80, 100, 120, and 140 mg/L at constant pH of 2, adsorption time of 90 min, and adsorbent of 1.25 g/L. As shown in Figure 9, the Cr(VI) ion adsorption decreases sharply from 97.5 to 62% as the concentration increased from 20 to 140 g/L for the BMNC; whereas, the adsorption decreased from 78 to 45.5% for BNa at similar concentrations. As the input ion concentrations increased, there are no proportionate active sites available at the constant adsorbent level [47]; alternatively, the adsorbents possess a fixed number of active sites, which become saturated above a certain concentration [48]. The graph suggests that 1.25 g/L of BMNC is capable of removing 98% of adsorbate Cr(VI) when the initial ion concentration is below 40 mg/L.

3.2.2. Parameters Interaction Effect and Optimization Using RSM-CCD. RSM is a statistical tool that is used to relate the independent variables with the response by generating a mathematical model [49, 50], and 3D response surface plots determine the significance of individual parameters and their interaction effects. The interaction effect was studied for four variables viz., adsorption time (60–120 min), pH (1.5–2.5), adsorbent (1–1.5 g/L), and Cr(VI) initial concentration (25–55 mg/L) on the removal efficiency. Thirty experimental runs were conducted for optimization and validation of the result, as listed in Table 4.

Model Fitting and ANOVA. A mathematical model relating the removal efficiency (%) response as a function of the independent parameters was developed using the Design-Expert software for the BMNC, which is shown in the quadratic model equation (11). The developed mathematical model was statistically evaluated to examine the significance of the model in terms of statistical factors such as probability (p value), coefficient of determination (R^2), and Fisher value (F value), as listed in Table 5. A model with $p < 0.05$ and R^2 close to unity indicates a significant model, and consequently, the response predicted by the model and the experimental results are close to each other. The quadratic model generated was found to be the best fit with $p < 0.0001$ and an $R^2 = 0.9969$:

$$\begin{aligned}\text{Removal efficiency}\,(\%) = {} & 96.5 + 1.61A - 2.52B + 0.442C \\ & - 3.95D + 0.967AB + 0.244AC \\ & + 1.1AD + 0.686BC - 0.492BD \\ & + 0.431CD - 2.706A^2 - 2.77B^2 \\ & - 1.17C^2 - 1.62D^2. \end{aligned} \quad (11)$$

Parameters like adsorption time, pH, and initial concentration with $p < 0.0001$ are significant, whereas the adsorbent dose with $p > 0.0001$ is not significant. Based on the ANOVA, the significant interactive terms are AB, AD, and BC with $p < 0.0001$; $p < 0.0507$, $p = 0.0007$, and $p = 0.002$ are respectively for AC, BD, and CD; hence, the latter three are not significant interaction terms. All the quadratic terms are significant with $p < 0.0001$.

The model's statistical significance is also indicated by R^2 values. For this model, both adjusted R^2 of 0.9941 and predicted R^2 of 0.9831 values are similar to R^2 of 0.9969. The actual and the predicted values involving four independent

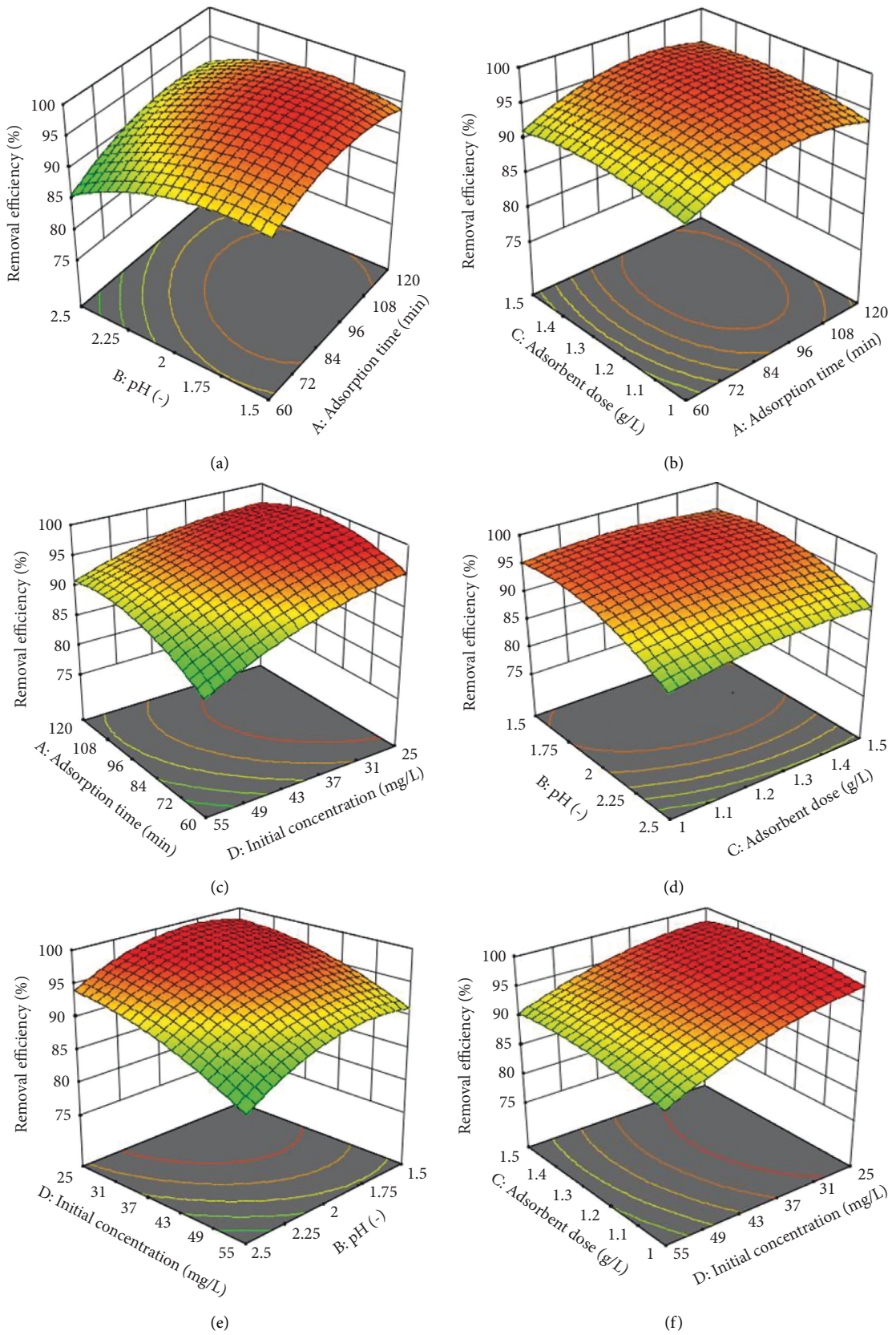

Figure 11: Interaction effect of (a) adsorption time vs. pH (adsorbent dose: 1.25 g/L, initial concentration: 40 mg/L), (b) adsorption time vs. adsorbent dose (pH: 2, initial concentration: 40 mg/L), (c) initial concentration vs. adsorption time (adsorbent dose:1.25 g/L, pH: 2), (d) pH vs. adsorbent dose (adsorption time:90 min, initial concentration: 40 mg/L), (e) pH vs. initial concentration (adsorption time:90 min,

Table 6: Working conditions of parameters and response for optimization.

Parameters	Goals	Lower Limits	Upper Limits
Adsorption time	In a range	60	120
pH	In a range	1.5	2.5
Adsorbent dose	In a range	1	1.5
Initial concentration	In a range	25	55
Removal efficiency	Maximize	76.5	97.9

process parameters and the design matrix are listed in Table 4.

A graph of actual experimental versus predicted values was plotted to correlate further the validity of the model. As shown in Figure 10 both the values are close to each other with an R-squared value of 0.9969. From this, it can be concluded that the developed model is significant to predict Cr(VI) removal efficiency by the BMNC.

Parameters' Interaction Effects on the Adsorption Process. The interaction effect of the adsorption time and pH on the Cr(VI) ion removal efficiency by the BMNC is shown in Figure 11. The response surface plot is shown in Figure 11(a) for removal efficiency as a function of adsorption time and pH at a given 1.25 g/L adsorbent concentration and 40 mg/L adsorbate concentration. It can be observed that the removal efficiency increases as the adsorption time increases from 60 to 110 min and as the pH decreases from 2.5 to 2. Beyond the adsorption time of 110 min and pH 2, the removal efficiency remains slightly constant.

Similarly, the response surface plot is shown in Figure 11(b) for removal efficiency as a function of adsorption time and adsorbent dose at the constant pH of 2 and initial Cr(VI) ions concentration of 40 mg/L. It can be observed that the removal efficiency increases as the adsorbent dose of 1 to 1.5 g/L and adsorption time of 60 to 110 min increase. However, it remains constant as time and adsorbent dose are further increased due to the Cr(VI) ions used up.

The interaction effect of contact time and initial Cr(VI) ion concentration on the removal efficiency by the BMNC is shown in Figure 11(c). The removal efficiency increases as the initial Cr(VI) decreases from 55 to 28g/L and contact time increases from 60 to 110 min. However, further increase in contact time and decrease in initial Cr(VI) concentration do not affect the removal efficiency. The decrease in removal efficiency with an increase in initial Cr(VI) concentration is due to the limited active sites at a 1.25 g/L adsorbent dose. As indicated from the model equation for the response variable, the combined effect of adsorption time and initial Cr(VI) concentration affects the removal efficiency positively with a coefficient of 1.1. This is also supported by the ANOVA result, which showed that the interaction of initial adsorbate concentration and adsorption time has a significant effect on the removal efficiency with $p < 0.0001$ (Table 5). Therefore, the interaction between contact time and initial adsorbate concentration has a significant effect on the removal efficiency of BMNC.

The combined effect of adsorbent dose and pH variations at a constant adsorption time of 90 min and initial Cr(VI) ion concentration of 40 mg/L is shown in the 3D graph in Figure 11(d). The removal efficiency increases as the pH is decreased from 2.5 to 2, but it declines beyond that. As the adsorbent dose increased from 1 to 1.25 g/L, the removal efficiency remains constant. As stated from the model equation, the combined effect of pH and adsorbent dose (BC) on the removal efficiency affects the response positively with a coefficient of 0.686. This interaction result is also supported by ANOVA, which has a significant effect on the removal efficiency by BMNC with $p < 0.0001$ (Table 5).

The 3D surface graph is shown in Figure 11(e), representing the interaction effect of pH and initial Cr(VI) adsorbate concentration on the removal efficiency by BMNC at a constant adsorption time of 90 min and adsorbent dose of 1.25 g/L. It was found that the removal efficiency increases as both pH and initial concentration decrease from 2.5 to 1.5 and 55 to 25 mg/L, respectively. The maximum removal efficiency was obtained at low pH and initial concentration. As indicated from the model equation for the response, the combined effect of pH and initial adsorbate concentration negatively affects the removal efficiency with a coefficient of −0.492. ANOVA results concur with these findings with $p < 0.0007$, as shown in Table 5, indicating there is no significant effect on the removal efficiency.

The interaction effect is shown in Figure 11(f) for the adsorbent dose and the initial concentration on the removal efficiency by the BMNC. The removal efficiency increases as the adsorbent dose increases from 1 to 1.5 g/L and as the initial adsorbate concentration decreases from 55 to 25 mg/L. As stated from the model equation for the response, the interaction effect of initial adsorbate concentration and adsorbent dose (CD) positively affects the removal efficiency with a coefficient of 0.431. This is also confirmed by the ANOVA result for the removal efficiency with $p < 0.0001$, as indicated in Table 5. The maximum removal efficiency was obtained at an initial Cr(VI) concentration of 40 mg/L and an adsorbent dose of 1.25 g/L.

Parameters Optimization and Validation. After the interaction effect of the adsorption, process variables have been studied, and optimization was carried out to determine the optimum conditions for the removal efficiency by BMNC. As discussed in previous section, the parameters have different effects on the removal efficiency (%). Response increases with adsorbent dose and time, whereas it decreases with initial concentration. Maximum adsorption efficiency was observed at pH of 2, whereas above this pH, it declines sharply. Table 6 lists the summary of optimization process conditions (lower and upper limits) of the parameters on the removal efficiency (%) response. A set of solutions was generated by the Design-Expert software to determine the optimum process parameters and selected based on high removal efficiency.

adsorbent dose:1.25 g/L), and (f) initial concentration vs. adsorbent dose (adsorption time: 90 min, pH: 2) on removal efficiency (%) response.

Table 7: Model predicted and experimental responses at optimum conditions.

Parameters	Adsorption time (min)	pH	Adsorbent dose (g/L)	Initial concentration (mg/L)	Removal efficiency (%)
Predicted	100.6	1.95	1.12	36.2	97.1
Observed	101	1.95	1.12	36.2	96.5

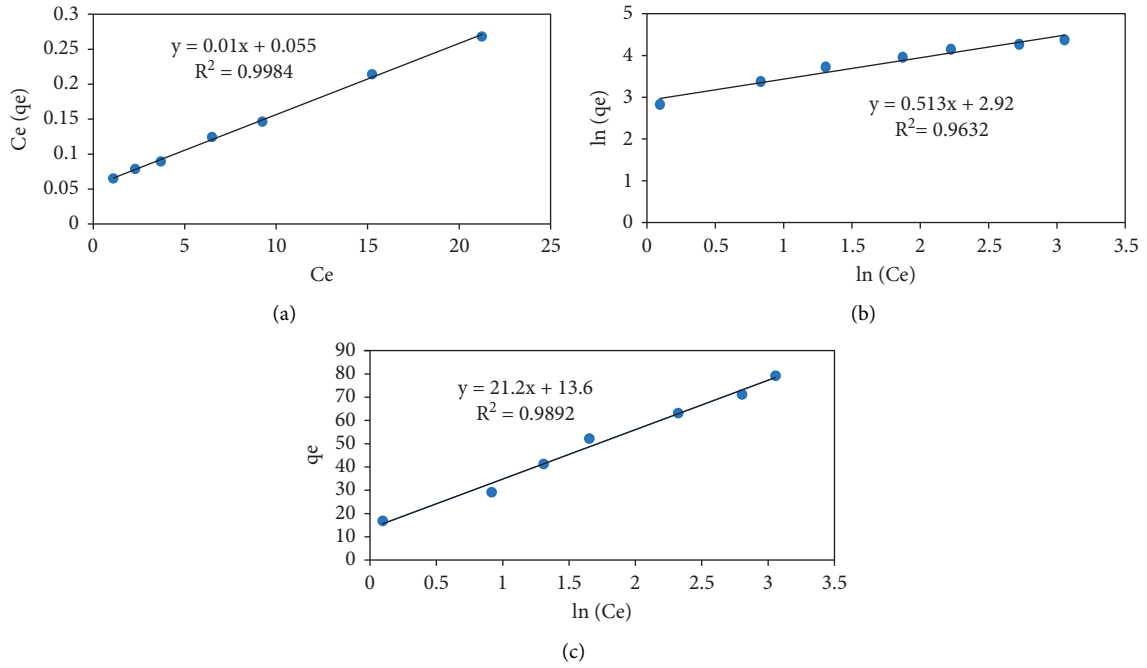

Figure 12: Langmuir (a), Freundlich (b), and Temkin (c) models for Cr(VI) ion adsorption by the nanocomposite adsorbent (BMNC).

Table 8: Parameters of isotherm models for Cr(VI) ion adsorption onto the nanocomposite adsorbent (BMNC).

Isotherm Models	Parameters	Values
Langmuir	Q_{max} (mg/g)	98.04
	R_L	0.133
	K_L (L/mg)	0.184
	$R2$	0.998
Freundlich	N	1.95
	Kf	18.6
	$R2$	0.963
Temkin	B	21.2
	K_T (L/mg)	1.9

Triplicate experiments were conducted to validate the optimized parameters, which are predicted by the model and numerical optimization. The removal efficiency obtained from the actual experiments was in close agreement with the predicted value by the model with a deviation of 0.674%, as listed in Table 7. Thus, the fitted model is significant and reliable to predict the response.

3.3. Adsorption Mechanisms

3.3.1. Study of Adsorption Isotherms. To study the adsorption isotherm, the initial concentration of Cr(VI) was varied at 20, 35, 50, 65, 80, 95, and 110 mg/L and allowed to be adsorbed on the surface of 0.112 g of BMNC; the final concentrations, equilibrium concentrations, and the capacity of the adsorbate at equilibrium were evaluated. Resulted data were then fitted to the models to observe which model best describes the adsorption process [15]. Langmuir model, Ce/qe, versus Ce data was plotted and the maximum adsorption capacity(Q_{max}, mg/g), the Langmuir equilibrium constant (K_L, L/mg), and the coefficient of determination (R^2) were determined from the curve fitting, as shown in Figure 12(a). In the same way, ln(Ce) versus ln(qe) data was plotted to see the fitness of the Freundlich model, and the coefficient of determination (R^2), the adsorption intensity (n), and other constants were determined from the fitted curve (Figure 12(b)). A graph of ln(Ce) versus q_e was plotted to see the fitness of the adsorption process to Temkin isotherm, as shown in Figure 12(c) and the values of B and K_T were calculated from the slope and intercept of the graph. Parameters evaluated from the isotherm models are summarized in Table 8. Based on the results, the removal efficiency by the BMNC, the coefficient of determination ($R^2 = 0.9984$) found by Langmuir is higher than those of the Freundlich ($R^2 = 0.9632$), and Temkin models ($R^2 = 0.989$). Thus, it can be deduced that monolayer adsorption was more effective than multilayer by adsorbate ions [35]. The maximum adsorption capacity of the Cr(VI) using the BMNC was found to be 98 mg/g. Since the value of R_L lies between 0 and 1, the Langmuir model was favourable in this

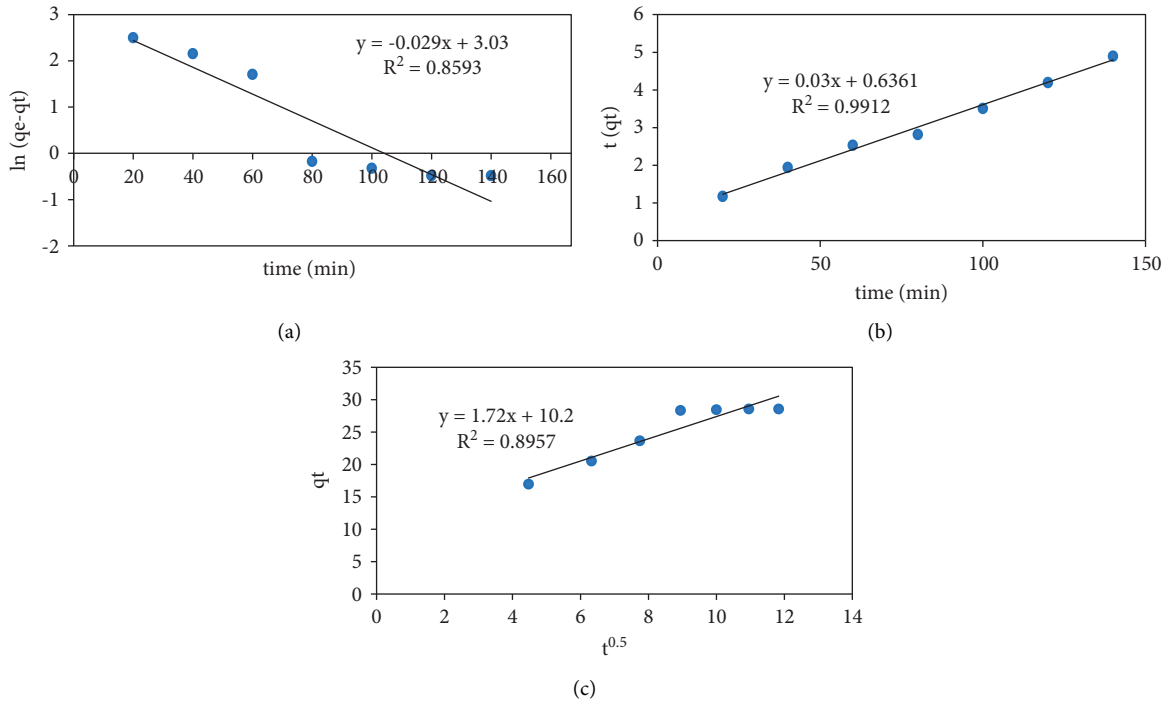

Figure 13: Pseudo-first-order (a), pseudo-second-order (b), and intraparticle diffusion (c) kinetic model plots.

Table 9: Parameters of kinetic models for Cr(VI) ion adsorption onto the nanocomposite adsorbent (BMNC).

Kinetic model	Parameters	Values
Pseudo-first order	qe (cal., mg/L)	29.2
	qe (exp., mg/L)	1.1
	K_1	0.029
	$R2$	0.859
Pseudo-second order	qe (cal., mg/L)	29.2
	qe (exp., mg/L)	33.7
	K_2	0.001
	$R2$	0.991
Intraparticle diffusion	K_d (mg/g.min$^{0.5}$)	1.72
	C (mg/g)	10.2

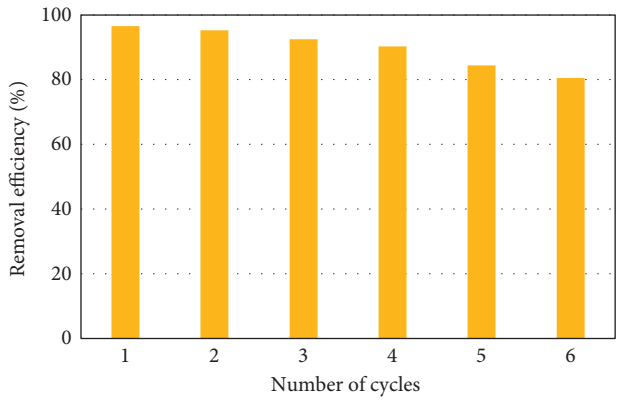

Figure 14: Regeneration and reuse of the nanocomposite adsorbent (BMNC) for Cr(VI) ions removal from water solution.

adsorption process [1]. As the value of n is greater than 1, the adsorption process is a physicochemical process [33].

3.3.2. Study of Adsorption Kinetics. To study the kinetics of adsorption by BMNC, pseudo-first-order, pseudo-second-order, and intraparticle diffusion models were examined and presented in Figure 13 and Table 9. Ln(qe−qt) versus adsorption time (t) was plotted to fit the data for the pseudo-first-order model. The coefficient of determination from the pseudo-first-order model was found to be 0.859, as it is shown in Figure 13(a). For the pseudo-second-order kinetic model, the data t/qt versus adsorption time was fitted and examined. The coefficient of determination was found to be 0.991, as shown in Figure 13(b). Similarly, qt versus $t^{0.5}$ was plotted to fit the data for the intraparticle diffusion kinetic model, as shown in Figure 13(c) and the values of K_d and C

Table 10: Comparison of the maximum adsorption (Q_{max}) capacity and removal efficiency of adsorbate Cr(VI) ions by different adsorbents.

Adsorbent	Optimum operating conditions	Remark	Reference
Chitosan/clay	Time: 60 min; pH: 2 Adsorbent dose: 2 g/L Initial concentration: 10 mg/L Removal efficiency: 94.3%	Fitted well with Langmuir isotherm model with Q_{max} of 80.31 mg/g and followed pseudo-second-order kinetic model	[24]
Acid and thermally modified bentonite clay	Time: 90 min; pH: 5 Adsorbent dose: 0.5 g/L Initial concentration: 30 mg/L Removal efficiency: 66%	Fitted well with Freundlich isotherm model with Q_{max} of 14.3 mg/g and follow pseudo-second-order kinetic model	[28]
Surfactant-modified bentonite	Time:120 min; pH: 3.4 Adsorbent dose: 0.44 g Concentration: 50 mg/L Removal efficiency: 93.2% Temperature: 25°C	Fitted well with Freundlich isotherm model with Q_{max} of 10 mg/g	[4]
Activated carbon from teff husk	Time: 2.07 hr; pH: 1.92 Initial concentration: 87.8 mg/L Adsorbent dose: 20.2 g/L Removal efficiency: 95.6%	Fitted well with Langmuir isotherm model and followed pseudo-second-order kinetic model	[15]
Fe_3O_4/bentonite	Time: 101 min; pH: 1.95 Initial concentration: 36.2 mg/L Adsorbent dose: 1.12 g/L Removal efficiency: 96.5%	Fitted well with Langmuir isotherm model with Q_{max} of 98 mg/g and followed pseudo-second-order kinetic model	This study

were calculated from the slope-intercept of the graph respectively. Hence, it can be deduced that the process of adsorption of the Cr(VI) ions onto BMNC is best fitted using the pseudo-second-order kinetics model. Here, the kinetics studies' results are similar to other literature on Cr(VI) ion removal using activated carbons and clay adsorbents [15, 33].

3.4. Recyclability of the BMNC. A study of recyclability has a huge significance to ensure the cost-effectiveness of BMNC and addressing environmental issues [44]. Figure 14 shows that the adsorption efficiency decreases slightly in each consecutive recycling step. This reduction from 96.4% in the first cycle to 80.5% in the sixth cycle can be due to the degradation of some adsorbent sites during these adsorption-desorption cycles and also some adsorption sites permanently occupied by solvent molecules [20]. Therefore, BMNC exhibits a good reusability potential since it removes adsorbate Cr(VI) ions over 80% from an aqueous solution even after six cycles.

3.5. Comparison of This Study with Some Previous Works. A comparison of the adsorption capacity and removal efficiency of variously reported adsorbents from previous literature is listed in Table 10, which is essential to put forward the significance of the BMNC.

4. Conclusions

A low-cost and naturally available bentonite-magnetite (Fe_3O_4) nanocomposite adsorbent (BMNC) was synthesized by the coprecipitation method under an inert N_2 gas atmosphere to examine Cr(VI) ions removal from water solutions. Characterization and analyses by AAS, DLS, BET, FTIR, SEM, and XRD confirmed the successful magnetite intercalation onto the bentonite clay. This magnetite nanoparticle intercalation is also confirmed as the specific surface area increases from 142 m^2/g to 177 m^2/g by BET analysis. DLS results show the 15 to 95 nm particle size distribution for BMNC. The magnetite intercalation into the bentonite enhanced the adsorption of Cr(VI) ions and also attributed magnetic properties, which aids the separation of the adsorbent from the solution easily using an external magnet. Adsorption time and adsorbent dose affect positively, whereas pH and initial concentration of Cr(VI) ions parameters affect negatively the adsorption removal process. RSM-CCD results in optimized parameters viz., adsorption time of 101 min, pH of 1.95, adsorbent dose of 1.12 g/L, and initial Cr(VI) concentration of 36.2 mg/L. Also, optimized

Cr(VI) ions removal of 96.5% was achieved from the water solution formulation by the BMNC. The maximum adsorption capacity from the Langmuir isotherm model was 98 mg/g, which indicates a monolayer adsorption nature. The adsorption kinetics suggests that the Cr(VI) ions by the BMNC were supported by a pseudo-second-order kinetic model. Regeneration studies indicate that the BMNC could easily be recovered using NaOH solution and Cr(VI) removal efficiency remained as high as 80% even after six cycles. This adsorbent developed from native bentonite clay is a potential alternative to mitigate the environmental concern particularly heavy metal ions from industrial wastewater effluents. Further desirable studies are column adsorption, removal of other heavy metal ions, thermodynamics, and industrial effluent treatment to affirm and maximize the removal efficiency and potential of the adsorbent.

Data Availability

The data used to support the findings of this research can be used to support the findings of the study is available within the article.

Conflicts of Interest

The authors declare that they have no conflicts of interest.

Authors' Contributions

Ngusey Adisu developed the methodology, collected the resources, and wrote the original draft; Subramanian Balakrishnan conceptualized the study, curated the data, validated the study, and wrote, reviewed, and edited the original draft; Haimanot Tibebe helped with software and carried out partial experiments

Acknowledgments

The authors would like to acknowledge the financial support from the Addis Ababa Science and Technology University for the experimental part of this research. .

References

[1] Y. Birhanu, S. Leta, and G. Adam, "Removal of chromium from synthetic wastewater by adsorption onto Ethiopian low-cost Odaracha adsorbent," *Applied Water Science*, vol. 10, no. 11, 2020.

[2] S. Pandey and J. Ramontja, "Recent modifications of bentonite clay for adsorption applications," *Focus on Sciences*, vol. 2, no. 4, pp. 1–10, 2016.

[3] P. Belibagli, B. Nur Ciftci, and Y. Uysal, "Chromium (Cr(VI)) removal from water with bentonite- magnetite nanocomposite using response surface methodology (RSM)," *Sigma Journal of Engineering and Natural Sciences*, vol. 38, no. 3, pp. 1217–1233, 2020.

[4] J. D. Castro-Castro, I. F. Macías-Quiroga, G. I. Giraldo-Gómez, and N. R. Sanabria-González, "Adsorption of Cr(VI) in aqueous solution using a surfactant-modified bentonite," *The Scientific World Journal*, vol. 2020, Article ID 3628163, 9 pages, 2020.

[5] M. Nur-E-Alam, M. A. S. Mia, F. Ahmad, and M. M. Rahman, "An overview of chromium removal techniques from tannery effluent," *Applied Water Science*, vol. 10, no. 9, pp. 205–222, 2020.

[6] T. Zhang, W. Wang, Y. Zhao et al., "Removal of heavy metals and dyes by clay-based adsorbents: from natural clays to 1D and 2D nano-composites," *Chemical Engineering Journal*, vol. 420, no. 2, Article ID 127574, 2021.

[7] S. Wu, J. Guo, Y. Wang, C. Huang, and Y. Hu, "Facile preparation of magnetic sodium alginate/carboxymethyl cellulose composite hydrogel for removal of heavy metal ions from aqueous solution," *Journal of Materials Science*, vol. 56, pp. 13096–13107, 2021.

[8] E. Alipanahpour Dil, M. Ghaedi, A. Asfaram, F. Mehrabi, and F. Sadeghfar, "Efficient adsorption of Azure B onto CNTs/Zn: ZnO@Ni2P-NCs from aqueous solution in the presence of ultrasound wave based on multivariate optimization," *Journal of Industrial and Engineering Chemistry*, vol. 74, pp. 55–62, 2019.

[9] S. Banuraman and T. P. Meikandaan, "Treatability study of tannery effluent by enhanced primary treatment," *International Journal of Modern Engineering Research*, vol. 3, no. 1, pp. 119–122, 2013.

[10] D. E. Kimbrough, Y. Cohen, A. M. Winer, L. Creelman, and C. Mabuni, "A critical assessment of chromium in the environment," *Critical Reviews in Environmental Science and Technology*, vol. 29, no. 1, pp. 1–46, 1999.

[11] M. D. Yahya, K. S. Obayomi, M. B. Abdulkadir, Y. A. Iyaka, and A. G. Olugbenga, "Characterization of cobalt ferrite-supported activated carbon for removal of chromium and lead ions from tannery wastewater via adsorption equilibrium," *Water Science and Engineering*, vol. 13, no. 3, pp. 202–213, 2020.

[12] M. S. Samuel, E. Selvarajan, R. Chidambaram, H. Patel, and K. Brindhadevi, "Clean approach for chromium removal in aqueous environments and role of nanomaterials in bioremediation: present research and future perspective," *Chemosphere*, vol. 284, Article ID 131368, 2021.

[13] K. H. Shah, S. Ali, M. Waseem et al., "Native and magnetic oxide nanoparticles (Fe_3O_4) impregnated bentonite clays as economic adsorbents for Cr (II) removal," *Journal of Solution Chemistry*, vol. 48, no. 11-12, pp. 1640–1656, 2019.

[14] S. Sobhanardakani, "Potential health risk assessment of heavy metals via consumption of caviar of Persian sturgeon," *Marine Pollution Bulletin*, vol. 123, no. 1–2, pp. 34–38, 2017.

[15] T. Adane, D. Haile, A. Dessie, Y. Abebe, and H. Dagne, "Response surface methodology as a statistical tool for optimization of removal of chromium (VI) from aqueous solution by Teff (Eragrostis teff) husk activated carbon," *Applied Water Science*, vol. 10, no. 1, pp. 37–13, 2020.

[16] V. Masindi, S. Foteinis, M. Tekere, and M. M. Ramakokovhu, "Facile synthesis of halloysite-bentonite clay/magnesite nanocomposite and its application for the removal of chromium ions: adsorption and precipitation process," *Materials Today Proceedings*, vol. 38, no. 2, pp. 1088–1101, 2021.

[17] V. B. Yadav, R. Gadi, and S. Kalra, "Clay based nanocomposites for removal of heavy metals from water: a review," *Journal of Environmental Management*, vol. 232, pp. 803–817, 2019.

[18] W. S. Chai, J. Y. Cheun, P. S. Kumar et al., "A review on conventional and novel materials towards heavy metal

adsorption in wastewater treatment application," *Journal of Cleaner Production*, vol. 296, Article ID 126589, 2021.

[19] S. Gu, X. Kang, L. Wang, E. Lichtfouse, and C. Wang, "Clay mineral adsorbents for heavy metal removal from wastewater: a review," *Environmental Chemistry Letters*, vol. 17, no. 2, pp. 629–654, 2019.

[20] P. Arabkhani and A. Asfaram, "Development of a novel three-dimensional magnetic polymer aerogel as an efficient adsorbent for malachite green removal," *Journal of Hazardous Materials*, vol. 384, Article ID 121394, 2020.

[21] J. Song, V. Srivastava, T. Kohout, M. Sillanpää, and T. Sainio, "Montmorillonite - anchored magnetite nanocomposite for recovery of ammonium from storm water and its reuse in adsorption of Sc^{3+}," *Nanotechnology for Environmental Engineering*, vol. 6, no. 3, 2021.

[22] P. Yuan, M. Fan, D. Yang et al., "Montmorillonite-supported magnetite nanoparticles for the removal of hexavalent chromium [Cr(VI)] from aqueous solutions," *Journal of Hazardous Materials*, vol. 166, no. 2-3, pp. 821–829, 2009.

[23] N. Belachew and G. Bekele, "Synergy of magnetite intercalated bentonite for enhanced adsorption of Congo red dye," *Silicon*, vol. 12, no. 3, pp. 603–612, 2020.

[24] A. E. Elsayed, D. Osman, s. Attia et al., "Synthesis of super magnetite (Fe_3O_4)/bentonite nanocomposite for efficient remediation for industrial wastewater effluents," *Egyptian Journal of Chemistry*, vol. 63, pp. 0–5026, 2020.

[25] V. Masindi and M. M. Ramakokovhu, "The performance of thermally activated and vibratory ball milled South African bentonite clay for the removal of chromium ions from aqueous solution," *Materials Today Proceedings*, vol. 38, no. 2, pp. 964–974, 2021.

[26] I. Wilson, "Applied Clay Mineralogy. Occurrences, processing and application of kaolins, bentonite, palygorskitesepiolite, and common clays," *Clays and Clay Minerals*, vol. 55, no. 6, pp. 644-645, 2007.

[27] P. P. Prabhu and B. Prabhu, "A review on removal of heavy metal ions from waste water using natural/modified bentonite," *MATEC Web of Conferences*, vol. 144, Article ID 02021, 2018.

[28] E. A. Ashour and M. A. Tony, "Ecofriendly removal of hexavalent chromium from aqueous solution using natural clay mineral: activation and modification effects," *SN Applied Sciences*, vol. 2, no. 12, Article ID 2042, 2020.

[29] J. Jia, Y. Liu, and S. Sun, "Preparation and characterization of chitosan/bentonite composites for Cr(VI) removal from aqueous solutions," *Adsorption Science and Technology*, vol. 2021, Article ID 6681486, 15 pages, 2021.

[30] J. Bayuo, K. B. Pelig-ba, and M. A. Abukari, "Optimization of adsorption parameters for effective removal of lead (II) from Aqueous Solution," *Physical Chemistry: An Indian Journal*, vol. 14, no. 1, pp. 123–147, 2019.

[31] K. K. Onchoke and S. A. Sasu, "Determination of hexavalent chromium (Cr(VI)) concentrations via ion chromatography and UV-vis spectrophotometry in samples collected from Nacogdoches wastewater treatment plant, east Texas (USA)," *Advances in Environmental Chemistry*, vol. 2016, Article ID 3468635, 10 pages, 2016.

[32] A. Wiryawan, R. Retnowati, and R. Y. P. Burhan, "Method of analysis for determination of the chromium (Cr) species in water samples by spectrophotometry with DPC," *Journal of Environmental Engineering & Sustainable Technology*, vol. 5, no. 1, pp. 37–46, 2018.

[33] R. Foroutan, S. J. Peighambardoust, R. Mohammadi, M. Omidvar, G. A. Sorial, and B Ramavandi, "Influence of chitosan and magnetic iron nanoparticles on chromium adsorption behavior of natural clay: adaptive neuro-fuzzy inference modeling," *International Journal of Biological Macromolecules*, vol. 151, pp. 355–365, 2020.

[34] H. T. Hii, "Adsorption isotherm and kinetic models for removal of methyl orange and remazol brilliant blue r by coconut shell activated carbon," *Tropical Aquatic and Soil Pollution*, vol. 1, no. 1, pp. 1–10, 2021.

[35] M. Hadi Dehghani, A. Zarei, A. Mesdaghinia, R. Nabizadeh, M. Alimohammadi, and M. Afsharnia, "Adsorption of Cr(VI) ions from aqueous systems using thermally sodium organobentonite biopolymer composite (TSOBC): response surface methodology, isotherm, kinetic and thermodynamic studies," *Desalination and Water Treatment*, vol. 85, pp. 298–312, 2017.

[36] K. Y. Foo and B. H. Hameed, "Insights into the modeling of adsorption isotherm systems," *Chemical Engineering Journal*, vol. 156, no. 1, pp. 2–10, 2010.

[37] M. Ghaedi, Z. Rozkhoosh, A. Asfaram, B. Mirtamizdoust, Z. Mahmoudi, and A. A. Bazrafshan, "Comparative studies on removal of Erythrosine using ZnS and AgOH nanoparticles loaded on activated carbon as adsorbents: kinetic and isotherm studies of adsorption," *Spectrochimica Acta Part A: Molecular and Biomolecular Spectroscopy*, vol. 138, pp. 176–186, 2015.

[38] H. Babas, G. Kaichouh, M. Khachani et al., "Equilibrium and kinetic studies for removal of antiviral sofosbuvir from aqueous solution by adsorption on expanded perlite: experimental, modelling and optimization," *Surfaces and Interfaces*, vol. 23, Article ID 100962, 2021.

[39] K. H. Shah, S. Ali, F. Shah et al., "Magnetic oxide nanoparticles (Fe_3O_4) impregnated bentonite clay as a potential adsorbent for Cr(III) adsorption," *Materials Research Express*, vol. 5, no. 9, Article ID 096102, 2018.

[40] K. Drobíková, K. Štrbová, M. Tokarčíková, O. Motyka, and J. Seidlerova, "Magnetically modified bentonite: characterization and stability," *Materials Today Proceedings*, vol. 37, no. 1, pp. 53–57, 2021.

[41] A. Kumar and P. Lingfa, "Sodium bentonite and kaolin clays: comparative study on their FT-IR, XRF, and XRD," *Materials Today Proceedings*, vol. 22, no. 3, pp. 737–742, 2020.

[42] M. Toor, B. Jin, S. Dai, and V. Vimonses, "Activating natural bentonite as a cost-effective adsorbent for removal of Congo-red in wastewater," *Journal of Industrial and Engineering Chemistry*, vol. 21, pp. 653–661, 2015.

[43] J. Lim, S. P. Yeap, H. X. Che, and S. C. Low, "Characterization of magnetic nanoparticle by dynamic light scattering," *Nanoscale Research Letters*, vol. 8, no. 1, p. 381, 2013.

[44] A. Maged, S. Kharbish, I. S. Ismael, and A. Bhatnagar, "Characterization of activated bentonite clay mineral and the mechanisms underlying its sorption for ciprofloxacin from aqueous solution," *Environmental Science and Pollution Research*, vol. 27, no. 26, pp. 32980–32997, 2020.

[45] K. H. Shah, S. Ali, M. Waseem et al., "Native and magnetic oxide nanoparticles (Fe_3O_4) impregnated bentonite clays as economic adsorbents for Cr (III) removal," *Journal of Solution Chemistry*, vol. 48, no. 11-12, pp. 1640–1656, 2019.

[46] E. Shabani, F. Salimi, and A. Jahangiri, "Removal of arsenic and copper from water solution using magnetic iron/bentonite nanoparticles (Fe_3O_4/bentonite)," *Silicon*, vol. 11, no. 2, pp. 961–971, 2019.

[47] A. A. Attia, S. A. Khedr, and S. A. Elkholy, "Adsorption of chromium ion (VI) by acid activated carbon," *Brazilian Journal of Chemical Engineering*, vol. 27, no. 1, pp. 183–193, 2010.

[48] A. A. El-Baz, I. Hendy, A. M. Dohdoh, and M. I Srour, "Adsorption of high chromium concentrations from industrial wastewater using different agricultural residuals," *Journal of Environmental Treatment and Techniques*, vol. 9, pp. 122–138, 2021.

[49] F. Ghorbani, S. Kamari, S. Zamani, S. Akbari, and M. Salehi, "Optimization and modeling of aqueous Cr(VI) adsorption onto activated carbon prepared from sugar beet bagasse agricultural waste by application of response surface methodology," *Surfaces and Interfaces*, vol. 18, Article ID 100444, 2020.

[50] S. U. Khan, D. T. Islam, I. H. Farooqi, S. Ayub, and F. Basheer, "Hexavalent chromium removal in an electrocoagulation column reactor: process optimization using CCD, adsorption kinetics, and pH modulated sludge formation," *Process Safety and Environmental Protection*, vol. 122, pp. 118–130, 2019.